Proceedings of ASME Turbo Expo 2004
Power for Land, Sea, and Air
June 14-17, 2004, Vienna, Austria

GT2004-53910

FOREIGN OBJECT DAMAGE BEHAVIOR OF A SiC/SiC COMPOSITE AT AMBIENT AND ELEVATED TEMPERATURES

Sung R. Choi, Ramakrishna T. Bhatt, J. Michael Pereira, and John P. Gyekenyesi
NASA Glenn Research Center, Cleveland, OH 44135, USA

ABSTRACT

Foreign object damage (FOD) behavior of a gas-turbine grade SiC/SiC ceramic matrix composite (CMC) was determined at 25 and 1316°C, employing impact velocities from 115 to 440 m/s by 1.59-mm diameter steel-ball projectiles. Two different types of specimen support were used at each temperature: fully supported and partially supported. For a given temperature, the degree of post-impact strength degradation increased with increasing impact velocity, and was greater in a partially supported configuration than in a fully supported one. The elevated-temperature FOD resistance of the composite, particularly under partially supported loading at higher impact velocities ≥ 350 m/s, was significantly less than the ambient-temperature counterpart, attributed to a weakening effect of the composite. For fully supported loading, frontal contact stress played a major role in generating composite damage; whereas, for partially supported loading, both frontal contact and backside bending stresses were combined sources of damage generation. The SiC/SiC composite was able to survive higher energy impacts without complete structural failure but suffered more strength affecting damage from low energy impacts than AS800 and SN282 silicon nitrides. [*Keywords*: SiC/SiC ceramic matrix composite; foreign object damage (FOD)]

INTRODUCTION

Ceramics, because of their brittle nature, are susceptible to localized surface damage and/or cracking when subjected to impact by foreign objects. It is also true that ceramic components may fail structurally even by soft particles when the kinetic energy of impacting objects exceeds certain limits. The latter case has been often found in aerospace engines in which combustion products, metallic particles or small foreign objects cause severe damage to blade/vane components, resulting in serious structural problems. Therefore, foreign object damage (FOD) associated with particle impact needs to be considered when ceramic materials are designed for structural applications. In view of this importance, a considerable amount of work on impact damage of brittle materials by sharp particles as well as by "blunt" particles or by plates has been accumulated both experimentally and analytically, including the assessments of FOD for turbine engine applications [1-14].

In previous studies [15-18], FOD behavior of two representative gas-turbine grade silicon nitrides, AS800 and SN282, was determined at ambient temperature using both flexure bars and disks. Fully supported ceramic target specimens were impacted at their centers by *steel ball projectiles* with a diameter of 1.59 mm in a velocity range from 220 to 440 m/s. AS800 silicon nitride exhibited a greater FOD resistance than SN282, due to its greater value of fracture toughness (K_{Ic}). The key material parameter, K_{Ic}, affecting FOD resistance was further evidenced by the FOD response of an additional equiaxed, fine-grained silicon nitride (NC132) that exhibited the lowest fracture toughness of the three silicon nitrides tested [16]. No single crack system was involved in impact event with increasing impact velocity, resulting in several different types of flaws associated individually or simultaneously. A fracture map was proposed to identify the occurrence of particular crack systems. The degree of damage was much more severe in thin biaxial disks than in flexure bars.

The current work, as an extension of the previous studies, investigates FOD behavior of a gas-turbine grade, silicon carbide fiber-reinforced silicon carbide (SiC/SiC). This 2-D woven SiC/SiC ceramic matrix composite has exhibited good elevated-temperature strength, creep and rupture properties and good thermal conductivity. However, like any other materials, there are a few of properties and behaviors that are required to be evaluated before the material is put into service. One of those properties and behaviors is how FOD affects the mechanical degradation of the composite at elevated temperatures close to typical operating or target temperatures of structural components. For this purpose, SiC/SiC CMC target specimens with a flexure bar configuration were impacted at velocities ranging from 115 to 440 m/s by 1.59-mm-diameter steel ball projectiles at both 25 and 1316°C. Two different types of specimen support, fully supported and partially supported, were used at each temperature. Post-impact strength of each target specimen impacted was determined in four-point flexure as a function of impact velocity to evaluate the severity of impact damage. Fractography was performed before and after post-impact strength testing to determine impact-damage morphologies.

EXPERIMENTAL PROCEDURES

Material and Test Specimens

The material used in this work was 2-D woven Sylramic, BN interface, melt-infiltrated SiC matrix composite. The CMC was fabricated by GE Power System Composites (Newark, DL). The detailed descriptions on the material and its processing can be found elsewhere [19]. Briefly, Sylramic fibers, produced in tow form by Dow Corning (Midland, MI) were woven into 2-D 5 harness-satin cloth and then converted to Sylramic iBN fibers. The Sylramic iBN cloth was cut into 230 x 150 mm plies, which were 8 ply-stacked and chemically vapor infiltrated with a thin BN-based interface coating followed by SiC matrix over-coating. Remaining matrix porosity was filled with SiC particulates and then with molten silicon at 1400°C. The SiC composite was composed of about 34 vol% SiC fibers, about 5 vol% BN coating, and about 61 vol% SiC coating, SiC particulates, and silicon. The nominal dimensions of each panel thus fabricated were about 230 mm by 150 mm with a thickness of about 2.4 mm. Typical SEM micrographs of the cross section of the composite are shown in Fig. 1 [20]. The panels were machined into thin flexure beams measuring 8 mm in width, 45 mm in length and 2.4 mm in as-furnished thickness.

Foreign Object Damage Testing

Foreign object damage (FOD) testing was carried out at both ambient and elevated temperatures using the experimental apparatus shown in Fig. 2. Detailed descriptions

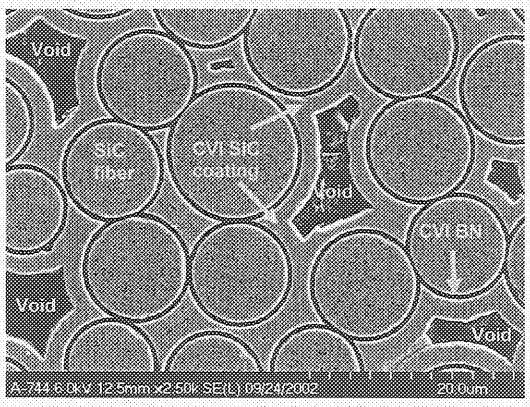

Figure 1. SEM micrograph of SiC/SiC ceramic matrix composite [20].

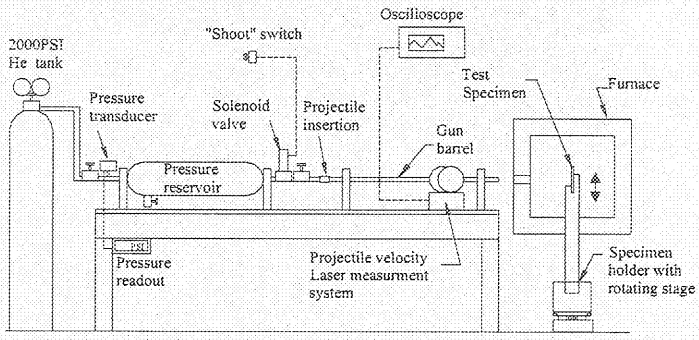

Figure 2. Impact testing apparatus with a high-temperature furnace [15].

of the apparatus can be found elsewhere [15-18]. Hardened (HRC≥60) chrome steel-balls with a diameter of 1.59 mm were inserted into a 300mm-long gun barrel with an inner diameter of 1.59 mm. A He-gas cylinder and relief valves were used to pressurize the reservoir to a specific level, depending on prescribed impact velocity. Upon reaching a specific level of pressure, a solenoid valve was instantaneously opened accelerating a steel-ball projectile through the gun barrel to impact a target specimen. The target specimen was fully or partially supported through a SiC specimen holder, as shown in Fig. 3. Each target specimen was aligned such that the projectile impacted at the center of the specimen with a normal incidence angle. Two different temperatures of 25 and 1316°C were used for each type of specimen support. In elevated-temperature testing, a target specimen was assembled together with a SiC holder outside of a furnace, and then the specimen-holder assembly was slowly (to minimize thermal shock) raised up via a DC servo motor

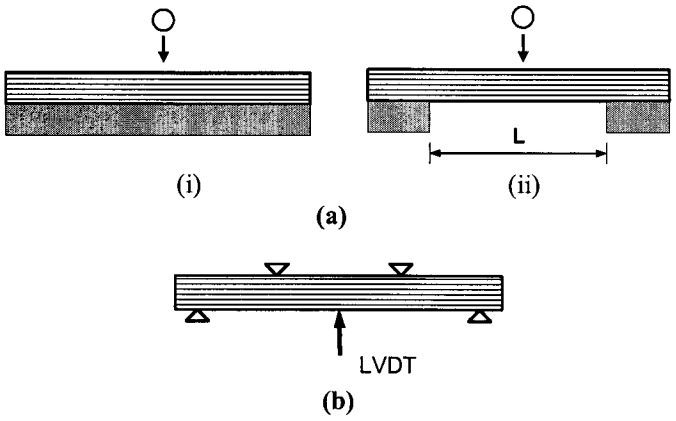

Figure 3. (a) Two types of target specimen support used in FOD testing: (a) (i) fully supported and (ii) partially supported (L=20 mm); (b) four-point flexure configuration used in post-impact strength testing, with an LVDT placed.

feed mechanism into the furnace whose temperature was slightly below the test temperature. The specimen was heated and held at the test temperature for about 15 min for thermal equilibration. A thermocouple was placed close to the target specimen to monitor and control temperature. After impact testing, the specimen was slowly lowered from the furnace and taken out of the holder assembly for further examination and testing.

Impact velocity of each projectile was determined using two pairs of laser transmitter and receiver, incorporated with two holes in the gun barrel, as described before [15-18]. The range of impact velocity employed in this work was from 115 to 440 m/s. At each temperature, one to three test specimens were used at each velocity for a given specimen support. Impact morphologies of target specimens were examined optically after impact testing.

Post-Impact Strength Testing

Strength testing for impacted target specimens was performed at ambient-temperature in air to determine the severity of impact damage using a four-point flexure fixture with 20-mm inner and 40-mm outer spans (see Fig. 3(b)). Each impacted specimen was loaded in the flexure fixture such that its impact site was subjected to tension within the inner span. An LVDT was used to determine the center deflection of specimens during strength testing. An electromechanical test frame (Model 8562, Instron, Canton, MA) was used in displacement control with an actuator speed of 0.5 mm/min. A fractographic analysis was performed after post-impact strength testing to determine failure origin, flaw configuration, and mode of fracture, if possible. 'As-received' flexural strength was also determined with three test

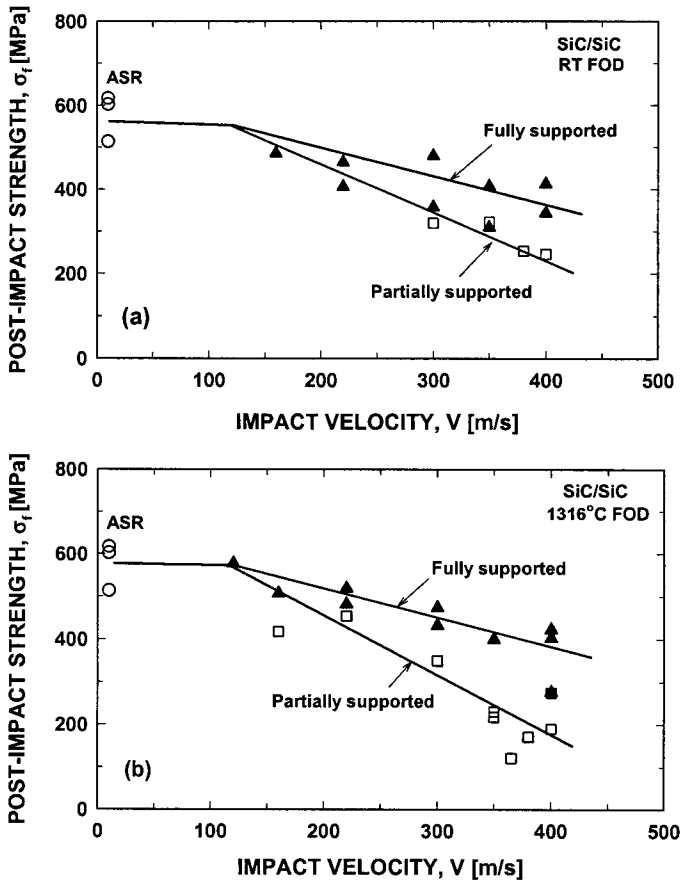

Figure 4. Post-impact flexural strength as a function of impact velocity, determined for SiC/SiC composite impacted by 1.59-mm-diameter steel ball projectiles with two different types of specimen support: (a) 25°C (RT) and (b) 1316°C. "ASR"=As-received strength determined at ambient temperature with no impact.

specimens using the same test fixture, test frame and test conditions that were utilized in the post-impact strength testing.

RESULTS AND DISCUSSION

Post-Impact Strength

The results of strength testing for impacted target specimens are shown in Fig. 4, where post-impact flexure strength was plotted as a function of impact velocity for both types of specimen support at each test temperature. Included in the figure is the as-received ('ASR') flexure strength (=578±56 MPa) determined at ambient temperature. One specimen at each temperature impacted at the lowest

velocity (i.e., 160 m/s at 25°C and 115 m/s at 1316°C) did not fracture from impact site because of negligible impact damage and its resulting strength was close to the as-received strength. As seen in the figure, post-impact strength decreased with increasing impact velocity at both temperatures, regardless of the type of specimen support, attributed to increased impact damage. For a given impact velocity, strength degradation was greater for the partially supported specimens than for the fully supported ones. The impact damage for the fully supported specimens was associated only with frontal contact stresses; while the damage for the partially supported ones resulted from both frontal contact and backside bending stresses, resulting in more significant strength degradation in the partially supported. Impact damage will be described in more detail in the next section.

As seen from the figure by comparison, the difference in strength between 25 and 1316°C was insignificant for the fully supported specimens. However, the size of frontal damage (i.e., 'spallation') was observed greater at 1316°C than at 25°C (as will be discussed later). This implies that the overall combined damage (fiber-matrix spallation, delamination, matrix/fiber cracking, etc.) that control strength would remain almost similar in severity at both temperatures for the fully supported configuration. By contrast, the strength difference between two temperatures was significant for the partially supported ones, particularly at higher impact velocities. Visual examinations of partially supported specimens showed that at higher velocities ≥ 350 m/s, appreciable damage such as deep spallation, cracking and backside delamination occurred at both front and backside of specimens. In some cases, a complete hole was formed through the thickness of a specimen. This predominant damage associated with partially supported specimens as well as a weakening effect of the composite at 1316°C gave rise to such a significant strength degradation.

Impact Morphology

The steel-ball projectiles were flattened or severely deformed upon impact at low impact velocities as a result of accompanying plastic deformation. At higher impact velocities (>300 m/s), the projectiles were subjected to both extreme heat evidenced by burning marks or fractured into many pieces. However, it was observed that the overall projectile damage was less in the current SiC/SiC composite than in AS800 and SN282 silicon nitrides [15-18], due to the fact that the SiC/SiC composite is less dense and 'soft' with a more open structure to give increased damping or energy absorbing capability.

The frontal impact damages generated in target specimens were indents, craters or deep holes with their size depending on impact velocity and temperature. Figure 5 shows the impact damage size (d) as function of impact velocity. The severity of damage increased with increasing impact velocity. For a given temperature, unlike strength, damage size was not sensitive to the type of specimen support either at 25 or at 1316°C. However, in terms of temperature, damage size was greater at 1316 than at 25°C, due to a temperature effect of the composite. As aforementioned, at higher impact velocities >350 m/s, backside damage became significant for the partially supported specimens with a presence of severe backside cracking and delamination due to backside tensile stresses. Typical examples showing impact damage for both fully and partially supported specimens are presented in Fig. 6. It should be noted that although not visible easily, the backside damage for the fully supported specimen was still significant, observed from its side view. The figure also includes the frontal damage site for each specimen. Schematic illustrations of progressive impact damage for both fully supported and partially supported loading are shown in Fig. 7. More detailed

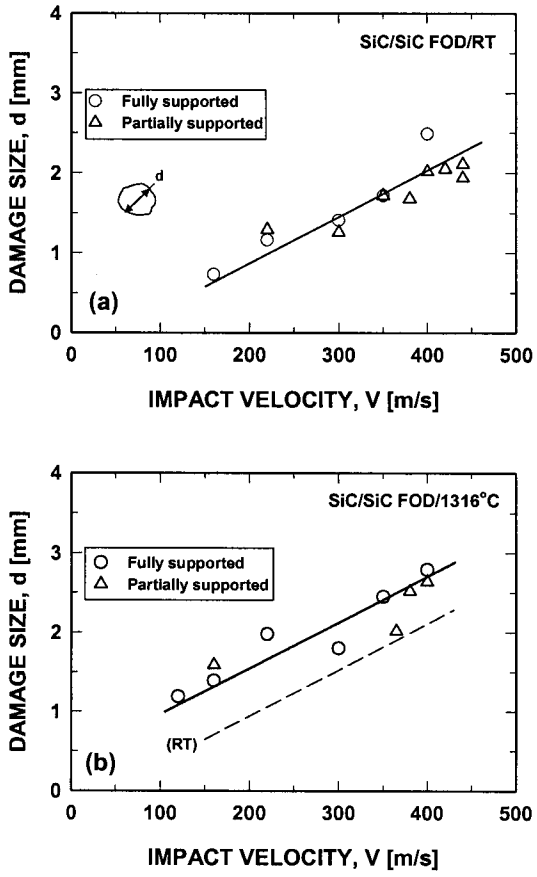

Figure 5. Frontal impact-damage size as a function of impact velocity for fully supported and partially supported specimens: (a) 25 (RT) and (b) 1316°C. The damage size (d) was an average of two diagonal measurements. The RT data in (a) is indicated as a dotted line in (b).

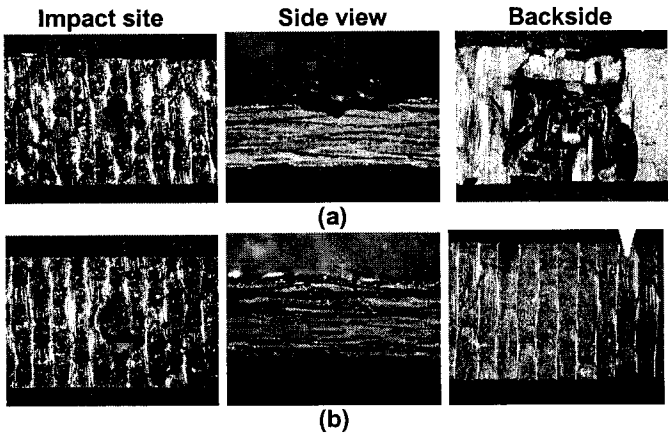

Figure 6. Typical examples of impact damage showing impact site, side, and backside of specimens impacted at 1316°C: (a) partially supported specimen impacted at 380 m/s; (b) fully supported specimen impacted at 400 m/s. Severe damage is observed from both side view and backside of the specimen in (a). Also note that backside delamination occurred in (b), viewed from a side view.

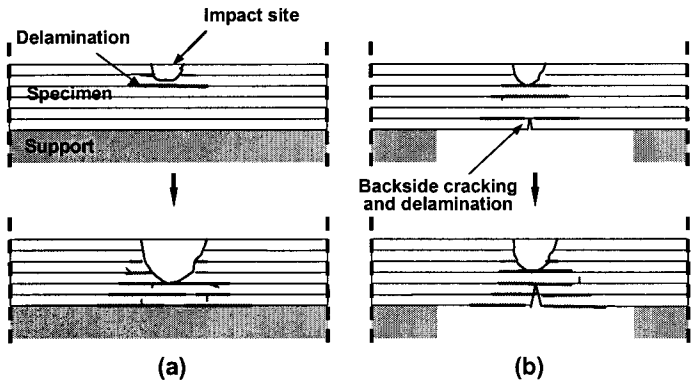

Figure 7. Schematics of impact damage associated with (a) fully supported and (b) partially supported specimen configurations. The vertical arrow indicates a case of increasing impact velocity.

and accurate analysis on impact damage and morphology should be done by appropriate methodologies. Optical examinations, in some or many cases, were not sufficient for the composite, in which NDE technique such as Computed Tomography (CT) must be employed to better characterize the degree and nature of damage [21]. The CT examination is in progress for damage assessment of the SiC/SiC specimens impacted.

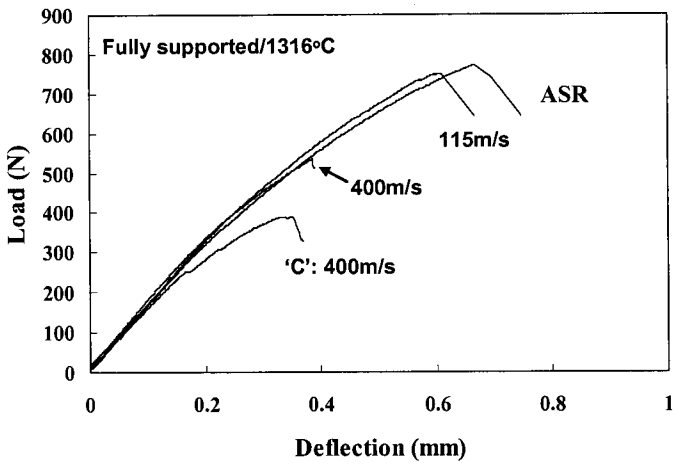

Figure 8. Typical load-deflection curves determined in flexure for fully supported specimens impacted at 1316°C with V = 115 and 400 m/s. The curve 'C' is for a specimen tested with its backside being placed in tensile stress. The peak load of each curve indicates a fracture load. "ASR"= As-received specimen tested at ambient temperature with no impact.

Load-Displacement Curves

Figure 8 shows typical load-deflection curves determined from flexure testing for fully supported specimens impacted at 115 and 400 m/s at 1316°C. Significant front and backside damage occurred for the specimens impacted at 400 m/s. The shape of curves remained almost unchanged until final fracture not only for the specimens impacted at a low velocity (=115 m/s) or a high velocity (=400 m/s) but for the as-received specimen ("ASR"). This indicates that the predominant damage induced at 400 m/s did not have any significant effect on flexural stiffness of the composite specimen. However, when a specimen with a similar degree of backside damage produced at 400 m/s was loaded reversely with the backside now subjected to tensile stress field, then the stiffness reduced significantly, also resulting in a low flexure strength (=276 MPa), as can be seen from the curve 'C'. This is, of course, indicative of the importance of the effect of loading geometry/configuration on composite stiffness as well as on post-impact strength.

Post-Impact Strength vs. Damage Size Relation

The relationship between post-impact strength and frontal damage size (d) is depicted in Fig. 9. The straight line indicates the best-fit with a slope of -0.5 in log (strength) and log (damage size). Except for two data points (arrowed) for the partially supported specimens at 1316°C that were severely

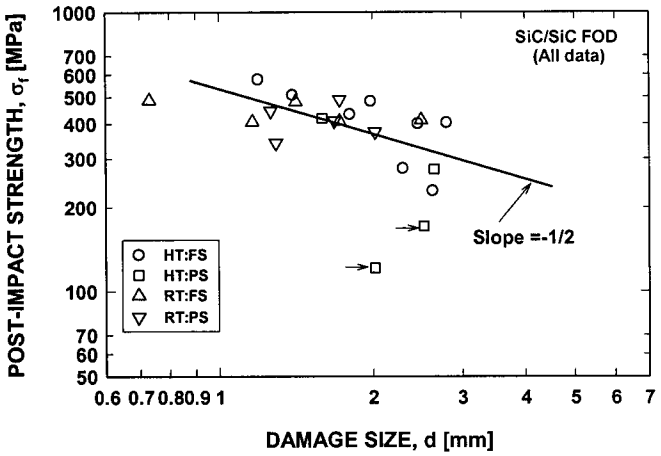

Figure 9. Post-impact strength as a function of frontal impact damage size. The best-fit line with a slope of -0.5 is included. HT: 1316°C; RT:25°C; FS: fully supported; PS: partially supported. The arrows indicate the specimens with significant backside damage.

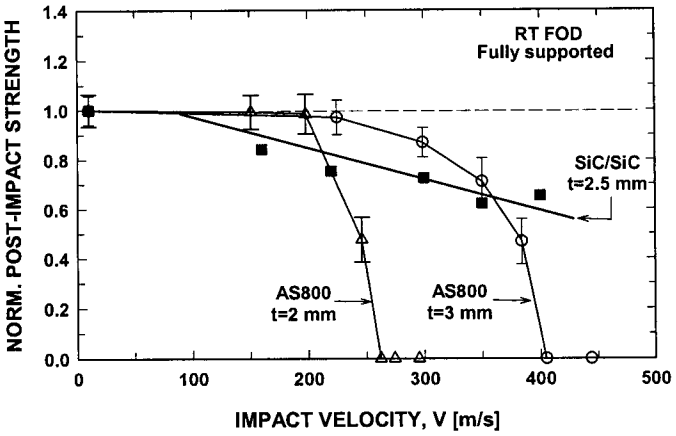

Figure 10. Comparison of normalized post-impact strength as a function of impact velocity between SiC/SiC composite and AS800 silicon nitride (two different thicknesses of t=2 and 3 mm)) [16], impacted in fully supported loading at 25°C.

damaged, the overall agreement of the slope with the experimental data was reasonable. Although it is not technically rigorous to apply the Griffith theory to this *continuous-fiber reinforced* composite and to these complex and random shapes of impact damage, the agreement seemed to follow the conventional strength-vs-damage relation. Use of the Griffith theory based on appropriate stress intensity factor (SIF) solutions together with the experimental data in Fig. 9 yields fracture toughness (K_{Ic}) as follows:

$$K_{Ic} \approx 10 - 15 \text{ MPa m}^{1/2}$$

The range between 10 and 15 MPam$^{1/2}$ indicates the results of use of different SIF solutions depending on various geometry factors. Although the use of fracture toughness for CMCs, instead of energy (e.g., work of fracture, etc), can be arguable, the value of K_{Ic} is still within the range that has been observed for several CMCs. This implies that the frontal impact damage size (d) would be an important contributor to determine the resulting post-impact strength of the composite even in the presence of appreciable delamination damage of layers.

Comparison in FOD between SiC/SiC Composite and Silicon Nitrides

Figure 10 shows a comparison in normalized post-impact strength between the current SiC/SiC composite and a gas-turbine grade silicon nitride, AS800. The post-impact strength of each material was normalized with respect to its respective unimpacted strength. The post-impact strength data for AS800 were determined in a flexure bar, fully-supported configuration with specimen thicknesses of t=2 and 3 mm, impacted by 1.6 mm steel ball projectiles at 25°C [15-18]. The critical impact velocity (V_c) in which test specimens fractured into two pieces upon impact was well defined for AS800 with $V_c \approx 260$ and 400 m/s, respectively, for t=2 and 3 mm. By contrast, such a critical impact velocity was not observed for the SiC/SiC composite. Hence, the SiC/SiC composite exhibited a much improved impact resistance over AS800 at higher impact velocities (V_c>220 and 350 m/s, respectively, compared with t=2 and 3 mm of AS800). A similar result was also observed from a previous study by van Roode et al. [11]. However, it must be noted that significant impact damage generated at high impact velocities, including impact holes, backside cracking and delamination etc, are still undesirable and must be avoided in view of performance, efficiency, structural integrity, and environmental stability. At lower impact velocities of $V_c \leq 200$ and ≤350 m/s, respectively, compared with t=2 and 3 mm of AS800, AS800 exhibited less strength affecting damage than the SiC/SiC composite.

Figure 11 shows normalized post-impact strength ($\bar{\sigma}_f$) as a function of kinetic impact energy (U_k) for the current SiC/SiC composite, AS800 and SN282 silicon nitrides [15-18]. A monotonic degradation in strength with increasing impact energy was typified for the SiC/SiC composite, yielding a linear relationship between log ($\bar{\sigma}_f$) and log (U_k). AS800 and SN282 silicon nitrides exhibited greater strength affecting damage at their respective impact energies of U_k>0.7 and <1.0J, compared with the SiC/SiC composite; whereas,

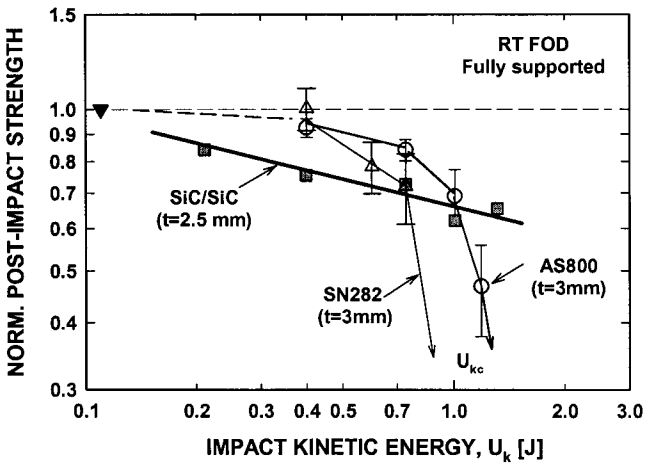

Figure 11. Comparison of normalized post-impact strength as a function of kinetic impact energy among SiC/SiC composite, AS800 and SN282 silicon nitrides [15,16], impacted in fully supported loading at 25°C. U_{kc}: critical impact energy.

the monolithic ceramics showed less strength affecting damage when U_k<0.7 and <1.0J. The best-fit equation for the composite was found to be as follows:

$$\bar{\sigma}_f = 0.66\, U_k^{-0.15} \qquad (1)$$

The Hertzian contact analysis for dense, brittle elastic solids gives the following equation [1]:

$$\sigma_f = \Phi''\, U_K^{-0.20} \qquad (2)$$

Although no physical evidence was provided in the current study, the SiC/SiC composite showed reasonable agreement in slope with the contact theory. The previous studies [15-18] indicated that the data for both AS800 and SN282 exhibited a significant deviation from the theory, as also can be seen from Fig. 11.

Factors of Consideration

Designing aeroengine components to withstand FOD events is a complex task. Consideration of many factors is required, both in the generation of FOD data as well as in actual component design efforts [22]. A sample of these numerous factors includes the following:

- Effect of projectile material/geometry
- Effect of test specimen material/geometry/architecture
- Effect of test-specimen support and component attachment
- Effect of temperature/environment
- Effect of FOD damage on continued exposure to elevated temperature and/or environment
- Appropriate protective coatings
- Geometrical design to enhance FOD resistance
- FOD/Reliability/Life prediction methodologies

Some of these factors are immediate subjects of study and the related work is under way, such as in the tasks reported in this paper. Others are long-term efforts and are pursued continually in the quest for improving the efficiency and reliability of aeroengine components. The way of specimen support, very important to affect overall FOD behavior, should be as realistic as possible to represent to actual attachment configurations. It has been experienced from this work that the complexity is more enormous in the SiC/SiC composite than in monolithic silicon nitrides in terms of basic understanding of impact damage and phenomenon.

CONCLUSIONS

1) The overall impact damage of the SiC/SiC composite was found to be greater for partially supported loading than for fully supported one at both 25 and 1316°C. The strength degradation with respect to impact velocity was more appreciable at 1316°C, particularly for partially supported loading at higher impact velocities.
2) For fully supported loading, frontal contact stresses played a major role in generating composite damage; whereas, for partially supported loading, both frontal contact and backside bending stresses were combined sources of damage generation.
3) Unlike AS800 and SN282 silicon nitrides, the SiC/SiC composite did not exhibit a critical impact velocity in which a target specimen fractures completely into two pieces. This indicates that enhanced FOD resistance could be achieved with the SiC/SiC composite particularly at higher impact velocities, as compared with the monolithic counterparts. However, the damage generated in the composite, particularly at >350 m/s, was still considered detrimental from a structural and component performance point of view.

Acknowledgements

The authors are thankful to R. Pawlik for the experimental work during the course of this study. This work was supported by the HOTPC and the UEET programs, NASA Glenn Research Center, Cleveland, Ohio.

REFERENCES

1. Wiederhorn, S. M., and Lawn, B.R., 1977, "Strength Degradation of Glass Resulting from Impact with Spheres," J. Am. Ceram. Soc., **60**[9-10], pp. 451-458.
2. Wiederhorn, S. M., and Lawn B. T., 1979, "Strength Degradation of Glass Impact with Sharp Particles: I, Annealed Surfaces," J. Am. Ceram. Soc., **62**[1-2], pp. 66-70.
3. Ritter, J. E., Choi,S. R., Jakus, K, Whalen, P. J., and Rateick, R. G., 1991, "Effect of Microstructure on the Erosion and Impact Damage of Sintered Silicon Nitride," J. Mater. Sci., **26**, pp. 5543-5546.
4. Akimune, Y, Katano, Y, and Matoba, K, 1989, "Spherical-Impact Damage and Strength Degradation in Silicon Nitrides for Automobile Turbocharger Rotors," J. Am. Ceram. Soc., **72**[8], pp. 1422-1428.
5. Knight, C. G., Swain, M. V., and Chaudhri, M. M., 1977, "Impact of Small Steel Spheres on Glass Surfaces," J. Mater. Sci., **12**, pp.1573-1586.
6. Rajendran, A. M., and Kroupa, J. L., 1989, "Impact Design Model for Ceramic Materials," J. Appl. Phys, **66**[8], pp. 3560-3565.
7. Taylor, L. N., Chen, E. P., and Kuszmaul, J. S., 1986 "Microcrack-Induced Damage Accumulation in Brittle Rock under Dynamic Loading," Comp. Meth. Appl. Mech. Eng., **55**, pp. 301-320.
8. Mouginot, R., and Maugis, D., 1985, "Fracture Indentation beneath Flat and Spherical Punches," J. Mater. Sci., **20**, pp. 4354-4376.
9. Evans, A. G., and Wilshaw, T. R., 1977, "Dynamic Solid Particle Damage in Brittle Materials: An Appraisal," J. Mater. Sci., **12**, pp. 97-116.
10. Liaw, B. M., Kobayashi, A. S., and Emery, A. G., 1984, "Theoretical Model of Impact Damage in Structural Ceramics," J. Am. Ceram. Soc., **67**, pp. 544-548.
11. van Roode, M., et al., 2002, "Ceramic Gas Turbine Materials Impact Evaluation," ASME paper no. GT2002-30505.
12. Richerson, D. W., and Johansen, K. M., 1982, "Ceramic Gas Turbine Engine Demonstration Program," Final Report, DARPA/Navy Contract N00024-76-C-5352, Garrett Report 21-4410.
13. Boyd, G. L., and Kreiner, D. M., 1987, "AGT101/ATTAP Ceramic Technology Development," Proceeding of the Twenty-Fifth Automotive Technology Development Contractors' Coordination Meeting, p.101.
14. van Roode, M., Brentnall, W. D., Smith, K. O., Edwards, B., McClain, J., and Price, J. R., 1997, "Ceramic Stationary Gas Turbine Development – Fourth Annual Summary," ASME paper no. 97-GT-317.
15. Choi, S. R., Pereira, J. M., Janosik, L. A., and Bhatt, R. T., 2002, "Foreign Object Damage of Two Gas-Turbine Grade Silicon Nitrides at Ambient Temperature," Ceram. Eng. Sci. Proc., **23**[3], pp. 193-202.
16. Choi, S. R., Pereira, J. M., Janosik, L. A., and Bhatt, R. T., 2002, "Foreign Object Damage Behavior of Two Gas-Turbine Grade Silicon Nitrides by Steel Ball Projectiles at Ambient Temperature," NASA/TM-2002-211821, National Aeronautics & Space Administration, Glenn Research Center, Cleveland, OH.
17. Choi, S. R., Pereira, J. M., Janosik, L. A., and Bhatt, R. T., 2003, "Foreign Object Damage of Two Gas-Turbine Grade Silicon Nitrides in a Thin Disk Configuration," ASME paper no. GT2003-38544.
18. Choi, S. R., Pereira, J. M., Janosik, L. A., and Bhatt, R. T., 2002, "Foreign Object Damage in Disks of Two Gas-Turbine Grade Silicon Nitrides by Steel Ball Projectiles at Ambient Temperature," NASA/TM-2003-212224, National Aeronautics & Space Administration, Glenn Research Center, Cleveland, OH.
19. Brewer, D., 1999, "HSR/EPM" Combustor Materials Development Program," Mat. Sci. Eng., **A 262**, pp. 284-291.
20. Bhatt, R. T., McCue, T. R., and DiCalo, J. A., 2003, "Thermal Stability of Melt Infiltrated SiC/SiC Composites," Ceram. Eng. Sci. Proc., **24**[4], pp. 295-300.
21. Bhatt, R. T., Choi, S. R., and Baaklini, G., "FOD Damage of EBC Coated SiC/SiC Composite," 2003, presented at the 5th PacRim Meeting, Nagoya, Japan.
22. Peralta and Yoshida, H., 2003, in Ceramic Gas Turbine Component Development and Characterization, van Roode, M, Ferber, M. K., and Richerson, D. W., eds., Vol. 2, pp. 665-692, ASME, New York, NY.